

# The Balloon-v1 Model for Metals With Improved Cyclic Response

Theodore L. Chang<sup>a,\*</sup>

<sup>a</sup>*IRIS Adlershof, Humboldt-Universität zu Berlin, Berlin, Germany, 12489.*

---

## Abstract

A versatile constitutive model is proposed for modelling complex cyclic response of metals. Within the framework of a revised subloading surface theory, the proposed model incorporates a novel isotropic hardening formulation based on the loading reversal information embedded in the normal yield ratio defined in the subloading surface theory. This formulation enables the model to capture a wide range of cyclic phenomena including cyclic hardening/softening, ratcheting, and stress relaxation under cyclic loading. The versatility of the proposed model is demonstrated through numerical examples involving various cyclic loading scenarios, and the results are compared with experimental data from the literature.

*Keywords:* constitutive modelling, plasticity, metal, ratcheting, cyclic response

---

## 1. Introduction

Predicting the constitutive behaviour of metals under cyclic loading poses a persistent difficulty in the field of solid mechanics. Regardless of their crystalline structure, metals demonstrate complex mechanical behaviour under repeated loading. These phenomena [1] include the Bauschinger effect, elastic/plastic shakedown, cyclic hardening or softening, and ratcheting. While conventional plasticity theory [see 2] adequately captures monotonic responses, it frequently lacks the fidelity required to predict these cyclic effects. Consequently, classical frameworks have been extended to establish a variety of advanced plasticity models capable of addressing these limitations.

Among these advanced approaches, two-surface formulations — specifically bounding surface theory [3, 4] and subloading surface theory [5–8] — have gained significant prominence. These frameworks have been successfully applied to a wide range of materials, including metals [e.g., 9, 10].

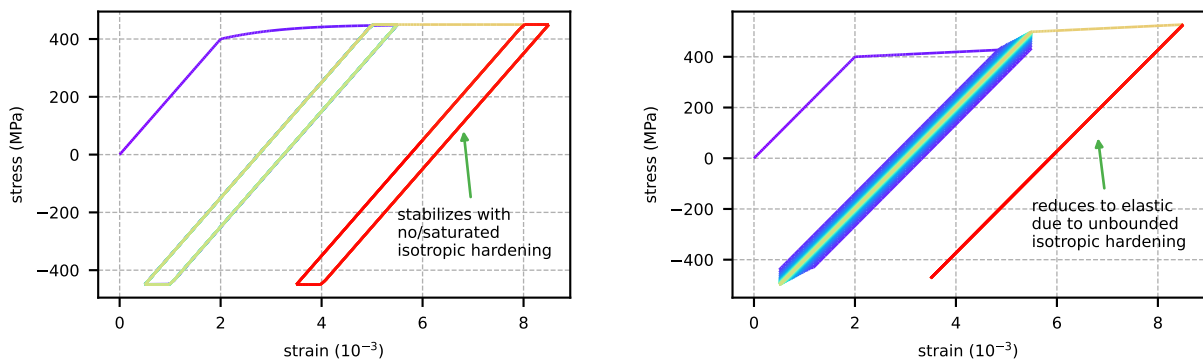
---

\*corresponding author

*Email address:* t1cfem@gmail.com (Theodore L. Chang)

25 Despite differences in nomenclature, the two theories share a fundamental basis, that is, both utilize  
 26 two evolving surfaces within stress space: an inner active surface enclosed by an outer bounding  
 27 surface. In both frameworks, the surfaces undergo isotropic and kinematic hardening, while the  
 28 evolution of the inner surface is governed by its proximity to the outer boundary. However, the  
 29 bounding surface theory [3, 10] is conceptually limited by its non-shrinking elastic domain/core,  
 30 which inhibits the accurate simulation of hysteresis during small one-sided cycles and prevents  
 31 the guarantee of smooth stiffness continuity at the elastic–plastic transition [11, see §8.2.3]. A  
 32 potential solution is to shrink the inner surface to a single point [12]. However, this eliminates the  
 33 possibility of introducing isotropic hardening, leaving all plastic phenomena to be captured solely by  
 34 kinematic hardening, which is not ideal since *‘the physical mechanism of isotropic hardening would  
 35 be different from that of the kinematic hardening’* [see 8, § 2.5]. In contrast, the subloading surface  
 36 theory successfully overcomes these issues while providing a more straightforward mathematical  
 37 framework and a much simpler numerical implementation [13].

38 Despite the benefits, its capability to describe all key cyclic phenomena is still subject to limita-  
 39 tions shared by other conventional and non-conventional plasticity models. For example, hysteresis  
 40 loops intrinsically lead to the accumulation of plastic strain, meaning plastic shakedown (the for-  
 41 mation of stable loops) requires that the active loading surface — whether the classical yield surface  
 42 or subloading surface — has saturated to a fixed size. This requirement stems from the theoretical  
 43 premise that *‘the (unbounded) isotropic hardening model suggests that the specimen will ‘shake  
 down’ to an elastic state’* [1, pg. 103]. This can be best demonstrated by the example depicted



(a) with a bounded isotropic hardening rule

(b) with an unbounded isotropic hardening rule

Figure 1: conventional isotropic hardening lacks flexibility in terms of capturing complex plastic phenomena

44

45 in Fig. 1, where the most elementary model [c.f., 2, § 1.2.2] is adopted with only isotropic hard-

46 ening defined. In Fig. 1a, an exponential saturation function (the Voce type) is used for isotropic  
47 hardening. Since it is bounded, the hysteresis loop eventually stabilizes under cyclic loading with  
48 fixed stress amplitudes, and once stabilized, it remains unchanged with further cycling, all plastic  
49 phenomena (e.g., ratcheting) can only be captured by others, such as kinematic hardening. In  
50 Fig. 1b, an unbounded linear function is used for isotropic hardening. In this case, the hysteresis  
51 loop continues to expand with further cycling, and eventually reduces to an elastic response.

52 However, experimental observations [e.g., 14–16] consistently show that continued cyclic hard-  
53 ening or softening can occur even after hysteresis loops have stabilized under fixed stress/strain  
54 amplitude cycling. Consequently, reproducing the full range of experimental results [e.g., 17–19]  
55 proves extremely challenging, if not impossible, without additional model refinements.

56 To simulate various cyclic phenomena, a mechanism that conditionally activates or deactivates  
57 isotropic hardening (a process also referred to as hardening stagnation, non-hardening region)  
58 must be introduced. Yoshida and Uemori [9, see, § 2.4] introduced an additional *non-isotropic-*  
59 *hardening* surface in the stress space, such that isotropic hardening can be activated or deactivated  
60 based on the size of the back stress, and thus the kinematic hardening. One should be aware  
61 that this approach does not work if kinematic hardening is not defined, although the absence of  
62 kinematic hardening is not practically useful. Despite this formulation is effective in certain cases,  
63 it still has limitations and cannot capture certain material behaviour [20]. Since the evolution of  
64 the back stress is ultimately driven by the plastic strain, such an approach can be equivalently  
65 formulated in the strain space. Hashiguchi et al. [7], Ohno [21], Chaboche [22] all adopt a strain  
66 space formulation. Such an approach is widely used in the literature as a basic building block for  
67 more complex models [see, e.g., 23–25]. Although recent efforts typically incorporate both isotropic  
68 and kinematic hardening [e.g., 26], improvements in cyclic response have often relied primarily on  
69 increasingly complex kinematic hardening rules [e.g., 27], also see the review by Kang [28].

70 In response to these challenges, the present work introduces a novel and efficient constitu-  
71 tive framework. This framework is achieved by incorporating a flexible isotropic hardening rule,  
72 grounded in the additive decomposition of plastic strain, with targeted enhancements to the  
73 subloading surface theory. The resulting model demonstrates the capability to accurately re-  
74 produce a broad spectrum of complex cyclic behaviour, including stable hysteresis loops, cyclic  
75 hardening or softening, and the previously intractable phenomenon of work hardening stagnation.

76 The rest of this paper is organised as follows. In § 2, we briefly summarise the general frame-  
77 work of subloading surface theory. In § 3, the proposed enhancements to the model are presented,  
78 including a split of plastic strain based on load reversals, a refined isotropic hardening rule that ac-  
79 counts for contributions from different plastic strain components, and other necessary modifications  
80 that further improve the model’s flexibility. In § 4, we first demonstrate the model’s capabilities  
81 through several simple examples, followed by a few more complex cases that simulate experimental  
82 results from the literature, demonstrating the effectiveness of the proposed model.

## 83 2. Background

84 To lay the foundation for subsequent discussions, we briefly summarise the general framework  
85 of subloading surface theory in this section, primarily following the formulation of Chang [13],  
86 which is more concise yet mathematically equivalent to the original by Hashiguchi et al. [7]. It  
87 should be noted that the notation system used in this work is *not* fully compatible with that of  
88 the previous work [13]. This section does not introduce any new concepts or formulations, which  
89 will be presented in the next section.

### 90 2.1. Basic Framework

#### 91 2.1.1. Constitutive Law

92 Based on the additive decomposition of deformation, conventional elasticity applies. That is,  
93 the stress tensor  $\boldsymbol{\sigma}$  can be expressed as the double contraction of the elasticity tensor  $\mathbf{D}_e$  and the  
94 elastic strain tensor  $\boldsymbol{\varepsilon}^e$ ,

$$\boldsymbol{\sigma} = \mathbf{D}_e : \boldsymbol{\varepsilon}^e = \mathbf{D}_e : (\boldsymbol{\varepsilon} - \boldsymbol{\varepsilon}^p), \quad (1)$$

95 where  $\boldsymbol{\varepsilon}$  is the total strain tensor and  $\boldsymbol{\varepsilon}^p$  is the plastic strain tensor.

#### 96 2.1.2. Subloading Surface

97 The subloading surface differs from the conventional yield surface by an additional scalar field  
98  $z$ , ranging from zero to unity, referred to as the normal yield ratio in the existing literature. It can  
99 be expressed as

$$f_s = \|\boldsymbol{\eta}\| - zF = \|\mathbf{s} - H_\alpha \boldsymbol{\alpha} + (z - 1) H_d \mathbf{d}\| - zF, \quad (2)$$

100 where  $\boldsymbol{\eta}$  is the shifted stress tensor,  $\boldsymbol{s} = \boldsymbol{s}(\boldsymbol{\sigma})$  is some measure of the stress tensor  $\boldsymbol{\sigma}$ , in von  
 101 Mises models, it is often taken as the deviatoric stress tensor  $\boldsymbol{s} = \text{dev}(\boldsymbol{\sigma})$ ,  $\boldsymbol{\alpha}$  is the back stress  
 102 tensor normalised by  $H_\alpha$ , and  $\boldsymbol{d}$  is the similarity tensor [13]. Both  $\boldsymbol{\alpha}$  and  $\boldsymbol{d}$  are internal history  
 103 variables that evolve in the stress space, with their magnitudes bounded by unity. Those two  
 104 tensors are further scaled by the scalar fields  $H_\alpha$  and  $H_d$  respectively, which may also evolve with  
 105 the development of plasticity. For simplicity,  $H_\alpha$  and  $H_d$  can be taken as fractions of  $F$ , a scalar  
 106 that characterises the size of the subloading surface and may be interpreted as the (reference) yield  
 stress. Fig. 2 presents a graphical illustration of each term. These two back stress like terms have

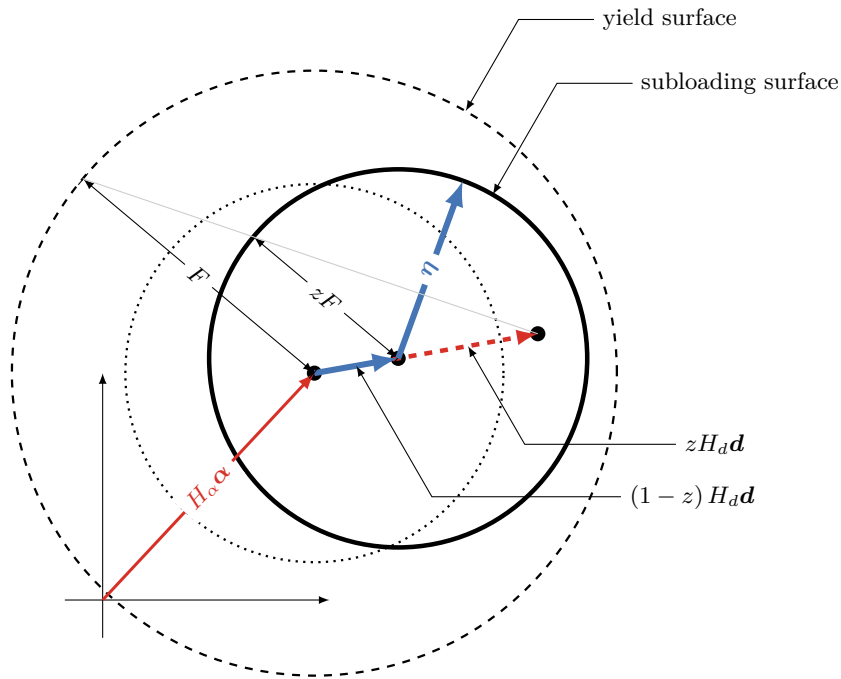


Figure 2: the subloading surface

107

108 different effects.

109 • The first term  $H_\alpha \boldsymbol{\alpha}$  is identical to the conventional back stress term, both  $\boldsymbol{\alpha}$  and  $H_\alpha$  evolve  
 110 with the accumulated plastic strain. As commonly understood, this term contributes to  
 111 kinematic hardening by shifting the center of the surface, and is primarily responsible for the  
 112 Bauschinger effect.

113 • The second term  $(1 - z) H_d \boldsymbol{d}$  has negligible influence during loading as  $z$  approaches unity.  
 114 However, during unloading, as  $z$  decreases, the center of the active plasticity surface is further

115 shifted away from  $H_\alpha \boldsymbol{\alpha}$ , thereby effectively enhancing the Bauschinger effect. This enables  
 116 the model to capture the so-called early re-yielding [14]. It also provides a mechanism to  
 117 control the amount of plastic strain accumulation during one-sided and small loading cycles.

118 One shall note that the normal yield ratio  $z$  serves a similar purpose to the variable  $\delta$  in bounding  
 119 surface formulations [3, 10]. Both variables quantify the proximity of the active plasticity surface  
 120 to a reference surface, though different terminologies are used in each formulation.

### 121 2.1.3. Flow and Evolution Rules

122 Assuming von Mises framework (thus  $\mathbf{s} = \text{dev}(\boldsymbol{\sigma})$ ) and associative plasticity, the flow rule takes  
 123 the following form,

$$\dot{\boldsymbol{\epsilon}}^p = \gamma \frac{\partial f_s}{\partial \boldsymbol{\sigma}} = \gamma \frac{\partial f_s}{\partial \boldsymbol{\eta}} : \frac{\partial \boldsymbol{\eta}}{\partial \boldsymbol{\sigma}} = \gamma \frac{\boldsymbol{\eta}}{\|\boldsymbol{\eta}\|} = \gamma \mathbf{n}, \quad (3)$$

124 where  $\gamma$  is the plastic multiplier. The scalar fields are driven by the accumulated plastic strain  $q$ ,  
 125 whose rate form is defined as a function of the plastic strain rate  $\dot{\boldsymbol{\epsilon}}^p$ . A common choice is to track  
 126 the magnitude of  $\dot{\boldsymbol{\epsilon}}^p$ , thus,

$$\dot{q} = \|\dot{\boldsymbol{\epsilon}}^p\| = \gamma. \quad (4)$$

127 For the yield function expressed in Eq. (2),  $\frac{\partial f_s}{\partial \boldsymbol{\sigma}}$  happens to be normalised. This is not always the  
 128 case for other yield criteria, where further normalisation may be required to obtain the simplifica-  
 129 tion  $\dot{q} = \gamma$ .<sup>1</sup> With the above, the following evolution rule is introduced for  $z$ ,

$$\dot{z} = U \dot{q}, \quad (5)$$

130 where  $U = U(z)$  is a function of  $z$ . Furthermore, the scalar bounds  $H_\alpha = H_\alpha(q)$ ,  $H_d = H_d(q)$  and  
 131  $F = F(q)$  are defined as functions of  $q$ . It is further required that  $H_d < F$  under all circumstances,  
 132 which ensures that the subloading surface is always inside the yield surface. The tensor fields  $\boldsymbol{\alpha}$

---

<sup>1</sup>Such normalisation is advantageous for both formulation and implementation: a) the increment  $\dot{q}$  does not depend on other tensors, making the computation of derivatives much simpler; and 2) the plastic multiplier  $\gamma$  is bounded, since  $\gamma = \|\dot{\boldsymbol{\epsilon}}^p\| \leq \|\dot{\boldsymbol{\epsilon}}\|$ , which can help stabilise the numerical implementation.

133 and  $\mathbf{d}$  evolve according to Armstrong–Frederick type rules [29], thus,

$$\dot{\boldsymbol{\alpha}} = b_{\alpha}(\mathbf{n} - \boldsymbol{\alpha})\dot{q}, \quad \dot{\mathbf{d}} = b_d(\mathbf{n} - \mathbf{d})\dot{q}, \quad (6)$$

134 where  $b_{\alpha}$  and  $b_d$  are material parameters controlling the rate of evolution. For the normalised back  
135 stress  $\boldsymbol{\alpha}$ , alternatively, the linear variant can also be adopted, for example,

$$\dot{\boldsymbol{\alpha}} = b_{\alpha}\mathbf{n}\dot{q}. \quad (7)$$

136 A combination of both types is also possible [e.g., 30].

### 137 **3. The Balloon-v1 Model**

138 In this section, we present a novel isotropic hardening rule based on the framework introduced  
139 in § 2, along with other relevant changes, to formulate a versatile constitutive model named as the  
140 Balloon-v1 model.

#### 141 *3.1. History of Load Reversals*

142 In conventional plasticity models, local reversals cannot be easily detected. A common criterion  
143 for detecting reversals is the double contraction  $\boldsymbol{\eta} : \dot{\boldsymbol{\eta}}$ . For example, in the multi-surface theory  
144 [31], the exact criterion is used to identify the initiation of a load reversal, which further controls  
145 the activation of a new surface.

146 The normal yield ratio  $z$  effectively represents the current ‘loading level’ at any given moment.  
147 By definition, this loading level is normalised between 0 and 1 thus does not depend on the current  
148 size of the yield surface: when it increases, the subloading surface expands, indicating a loading  
149 process; when it decreases, the subloading surface contracts, indicating an unloading process. Thus,  
150 load reversals can be detected with ease by checking whether  $z$  ever decreases within the given  
151 (sub-)step.

152 For a material (point) that has experienced up to  $N$  load reversals, let the normal yield ratio  
153 at each load reversal be denoted as  $z_r^j$  with  $j = 1, 2, 3, \dots, N$  standing for the  $j$ -th reversal. The  
154 initial value, if required, can be set to zero:  $z_r^0 = 0$ . We use  $z_r$  to denote some measure of the

155 entirety of  $z_r^j$ , thus,

$$\boxed{z_r = Z \left( \left\{ z_r^j \right\}_{j=0}^N \right) = Z \left( z_r^0, z_r^1, z_r^2, \dots, z_r^N \right).} \quad (8)$$

156 In the above,  $Z(\cdot)$  is a function that maps the collection  $\{z_r^j\}_{j=0}^N$  to a single scalar  $z_r$ . Depending  
 157 on the specific choice of function  $Z$ ,  $z_r$  embodies different memory effects. For example,  $z_r$  can  
 158 take the maximum/minimum value of the most recent  $M$  values. When  $M = 1$ ,  $z_r$  is the most  
 159 recent value  $z_r^N$ . When  $M \geq N$ ,  $z_r$  is simply the maximum/minimum value of all  $z_r^j$ . By such an  
 160 ansatz, it is effectively assumed that the material has a limited memory of load reversals. Since  
 161 by definition  $z$  is the ratio between the size of the current subloading surface and that of the yield  
 162 surface, stress information is inherently embedded in  $z$ , thus  $z_r$ . This allows one to account for  
 163 some key parameters such as stress magnitude and mean stress (of the cyclic loading protocol) in  
 164 a either direct or indirect way. For brevity, we do not explore different possibilities in this work.

### 165 3.2. Additive Decomposition of Plastic Strain

166 It is possible to split the plastic strain  $\epsilon^p$  into at least two parts,

$$\epsilon^p = \epsilon_m^p + \epsilon_c^p + \dots, \quad (9)$$

167 with  $\epsilon_m^p$  denoting the ‘monotonic’ part and  $\epsilon_c^p$  denoting the ‘cyclic’ part. The rationale behind  
 168 this split is straightforward: the accumulated plastic strain  $q$  defined in Eq. (4) only tracks the  
 169 total amount of plastic deformation, although it is non-decreasing, there is no way to infer further  
 170 details of the corresponding loading process. As also investigated by Meyer and Ahlström [20],  
 171 experiments show that  $q$  alone ‘cannot describe the axial yield stress evolution’ for certain types of  
 172 metals. The split Eq. (9) allows one to distinguish between the plastic strain accumulated during  
 173 monotonic loading (according to an appropriate definition of ‘monotonic’) and that accumulated  
 174 during load reversals. This distinction makes it possible to account for various microstructural  
 175 effects, such as the rearrangement/annihilation of dislocations. It is reasonable to assume that  
 176 the plastic strain increment  $\epsilon^p$  within a given (sub-)step would be distributed between two parts  
 177 according to some rule, which may depend on the current loading level  $z$ , and/or its history  $z_r$ .

178 Without loss of generality, one can then define

$$\dot{\boldsymbol{\varepsilon}}_m^p = K_m \dot{\boldsymbol{\varepsilon}}^p, \quad \dot{\boldsymbol{\varepsilon}}_c^p = K_c \dot{\boldsymbol{\varepsilon}}^p, \quad (10)$$

179 where  $K_m = K_m(z, z_r)$  and  $K_c = K_c(z, z_r)$  are functions of  $z$  and  $z_r$  (or equivalently,  $\{z_r^j\}_{j=0}^N$ ) that  
 180 yield ratios between zero and unity. It is possible to further impose the constraint  $K_m + K_c = 1$   
 181 such that there are exactly two components  $\boldsymbol{\varepsilon}^p = \boldsymbol{\varepsilon}_m^p + \boldsymbol{\varepsilon}_c^p$ , however, this is not strictly necessary.  
 182 A similar split can be applied to  $q$  such that

$$\boxed{\dot{q}_m = K_m \dot{q}, \quad \dot{q}_c = K_c \dot{q}.} \quad (11)$$

183 It is possible to propose a more sophisticated definition of  $K_m$  that may further account for  
 184 other history variables, such as plastic strain. We are refrained from doing so in this work to keep  
 185 the formulation simple.

### 186 3.3. Proposed Isotropic Hardening

187 With Eq. (11), the isotropic bound  $F$  can be defined as a function of both  $q_m$  and  $q_c$  instead  
 188 of  $q$  alone. Assuming an additive decomposition, it can be expressed as

$$F = F_m + F_c. \quad (12)$$

189 In the following, we elaborate the two components  $F_m$  and  $F_c$  and their effects on isotropic hard-  
 190 ening respectively.

#### 191 3.3.1. Work/Isotropic Hardening Stagnation

192 The most distinctive feature of the subloading surface theory is that the normal yield ratio  $z$   
 193 gradually approaches unity from zero during the loading process. Thus, there is no elastic region  
 194 during this process, as  $z$  accumulates with plastic deformation since it is driven by  $q$  as defined in  
 195 Eq. (5). Eq. (5) can be rearranged and integrated to obtain the change of  $q$  due to the change of  
 196  $z$ , say, for example, from  $z = 0$  to some  $z = z^* < 1$ ,

$$\Delta q = \int_0^{z^*} \frac{1}{U} dz. \quad (13)$$

197 Noting that regardless of the specific form of  $U(z)$ , the right-hand side is always deterministic (a  
 198 constant), meaning that loading from  $z = 0$  to  $z = z^*$  always requires the same amount of plastic  
 199 strain accumulation  $\Delta q$ .

200 Due to this deterministic mapping between  $\Delta z$  and  $\Delta q$ , those aforementioned strain space  
 201 formulations for isotropic hardening stagnation can be equivalently reformulated in the  $z$  space,  
 202 thus the stress space. We assume

$$F_m = F_m(q_m) \tag{14}$$

203 is a function of  $q_m$  solely. By choosing a proper  $K_m$ , for example,  $K_m = 0$  for  $0 \leq z \leq z_r$ , it is  
 204 possible to fully deactivate the evolution of  $q_m$ , thus  $F_m$ , during cyclic loading phase.

205 This type of stagnation is similar to the approach proposed by Ucak and Tsopelas [32, 33], who  
 206 used a certain set of criteria based on the same memory surface [21] to distinguish between two  
 207 distinct regions/phases: the plateau region where isotropic hardening stagnates, and the hardening  
 208 region where isotropic hardening evolves normally. A recent application of this idea can be found  
 209 in the work by Hu et al. [34]. Unlike existing formulations, the proposed approach Eq. (14) requires  
 210 no additional history variables for a secondary surface (whether defined in stress or strain space).  
 211 Similar information has already been inherently embedded in  $z$ . Furthermore, because  $z$  is a scalar,  
 212 it avoids tensor bookkeeping and yields a simpler, more efficient implementation. Finally, because  
 213  $K_m$  is a continuous function, when  $z$  gradually increases, it can be gradually (re-)activated from a  
 214 partially or fully deactivated state.

### 215 3.3.2. Cyclic Hardening/Softening

216 The cyclic hardening/softening is controlled by  $F_c$ , which is assumed to be governed by the  
 217 following evolution rule,

$$\boxed{\dot{F}_c = b_f (H_c - F_c) \dot{q}_c \quad \text{with} \quad H_c = H_c(q_m)} \tag{15}$$

218 In the above,  $b_f$  is a material parameter that controls the rate of saturation, and  $H_c$  is the saturation  
 219 value that may depend on  $q_m$ . It is possible to associate  $H_c$  with  $F_m$  such that the former is a  
 220 fraction of the latter. With the evolution of  $q_c$ ,  $F_c$  would gradually saturate to  $H_c$ . Meanwhile,  
 221 since  $H_c = H_c(q_m)$  depends on  $q_m$ , it would also evolve during monotonic loading phases. Eq. (15)

222 thus allows multi-stage saturation that allows cyclic hardening/softening under various loading  
 223 histories. This differs from other models in the literature [e.g., 21, 25] in which similar saturation  
 224 can only occur once.

### 225 3.3.3. Other Relevant Changes

226 With Eq. (12), the size of the subloading surface (isotropic hardening) is bounded by  $F_m + H_c$   
 227 which is governed by  $q_m$  solely. Stable hysteresis loops would eventually saturate  $F$  to this value  
 228 via the accumulation of  $q_c$ . In principle, a similar definition can be applied to bounds  $H_\alpha$  and  $H_d$ .  
 229 However, there is no strong experimental evidence indicating that these bounds exhibit hardening  
 230 or softening behaviour. To avoid unnecessary complexity, they are defined solely as functions of  
 231  $q_m$ , i.e.,  $H_\alpha = H_\alpha(q_m)$  and  $H_d = H_d(q_m)$ .

### 232 3.4. Objective Transition

233 As shown in Eq. (13), for a given interval of  $z$ , the corresponding change in  $q$  is always constant,  
 234 regardless of the specific form of  $U(z)$  — as long as it is given. However,  $z$  only measures the relative  
 235 loading level. As a result, the response curve becomes steeper when the yield stress is larger, and  
 236 less so when it is smaller. To make this transition more objective and less dependent on material  
 237 parameters, we propose the following revision.

$$\boxed{\dot{z} = \frac{U}{F}\dot{q}.} \quad (16)$$

238 Furthermore, in earlier models [8, 13], the function  $U$  does not consider loading history. It is  
 239 further extended in this work to account for loading history by introducing the dependence on  $q_m$ .  
 240 Thus,  $U = U(q_m, z)$ . A typical choice can be

$$U(q_m, z) = -u \ln z \quad (17)$$

241 with  $u = u(q_m)$  being a varying parameter that gradually decreases with  $q_m$  instead of a constant.  
 242 Or, following the suggestion by Chang [13], a power function can be used,

$$U(q_m, z) = u(z^{-n} - 1) \quad \text{for} \quad 0 < n \leq 1, \quad (18)$$

243 again, with  $u = u(q_m)$ .

244 3.5. Choice of  $K_m$  and  $K_c$

245 As explained earlier, the introduction of  $z_r$  allows one to identify two distinct loading phases:  
 246 monotonic loading when  $z$  increases from  $z_r$  to 1, and cyclic loading when  $z$  increases from 0 to  $z_r$ .  
 247 The split functions  $K_m$  and  $K_c$  shall meet the following requirements.

- 248 1. For  $0 \leq z < z_r$ ,  $\dot{q}$  mostly distributes to  $\dot{q}_c$ .
- 249 2. For  $z_r \leq z \leq 1$ ,  $\dot{q}$  mostly distributes to  $\dot{q}_m$ .
- 250 3. The amount of  $\dot{q}_m$  accumulated during cyclic loading phase shall be inversely proportional  
 251 to  $z_r$ .

252 To fulfil these, the following expression is chosen for  $K_m$  in this work.

$$K_m = \begin{cases} 0, & 0 \leq z < z_r, \\ 1 - \exp\left(\frac{z - z_r}{k_r(z - 1)}\right), & z_r \leq z \leq 1, \end{cases} \quad (19)$$

253 in which  $k_r$  is a material parameter that controls the transition. Eq. (19) provides a smooth  
 transition of  $K_m$  from zero at  $z = z_r$  to unity at  $z = 1$ . The function is illustrated in Fig. 3. It is

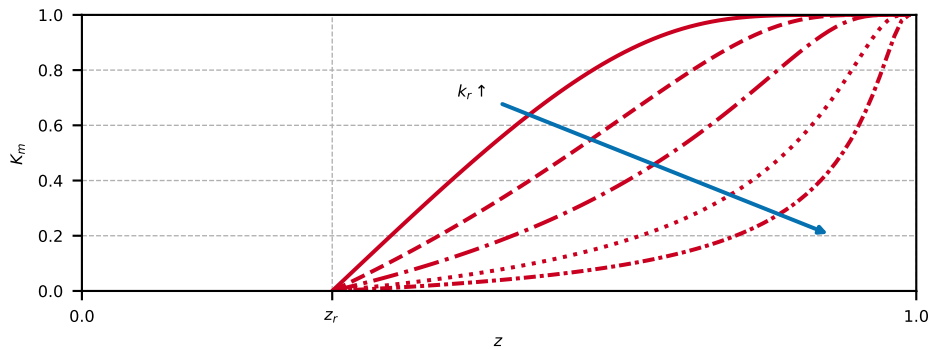


Figure 3: illustration of  $K_m$  defined in Eq. (19)

254

255 assumed that  $K_c = 1 - K_m$ .

256 3.6. Summary

257 The proposed formulation is summarised in Table 1. It should be emphasised that the for-  
 258 mulation presented in this work is general. For specific applications, minor changes, for example,  
 259 accounting for extra constants  $\sqrt{\frac{2}{3}}$  in von Mises models [see 13], may be made. For scalar bounds

Table 1: summary of the proposed formulation

Constitutive Law	$\boldsymbol{\sigma} = \mathbf{D}_e : (\boldsymbol{\varepsilon} - \boldsymbol{\varepsilon}^p)$
Subloading Surface	$f_s = \ \boldsymbol{\eta}\  - zF$ $F = F_m + F_c$ $\boldsymbol{\eta} = \mathbf{s} - H_\alpha \boldsymbol{\alpha} + (z - 1) H_d \mathbf{d}$
Flow Rule	$\dot{\boldsymbol{\varepsilon}}^p = \gamma \mathbf{n} = \gamma \frac{\boldsymbol{\eta}}{\ \boldsymbol{\eta}\ }$
Evolution Rules	$\dot{q} = \gamma$ $F\dot{z} = U\dot{q}$ $\dot{q}_m = K_m \dot{q}$ $\dot{F}_c = b_f (H_c - F_c) K_c \dot{q}$ $\dot{\boldsymbol{\alpha}} = b_\alpha (\mathbf{n} - \boldsymbol{\alpha}) \dot{q}_m$ $\dot{\mathbf{d}} = b_d (\mathbf{n} - \mathbf{d}) \dot{q}_m$

260  $H_\alpha = H_\alpha(q_m)$ ,  $H_d = H_d(q_m)$ ,  $H_c = H_c(q_m)$  and  $F_m = F_m(q_m)$ , any suitable univariate functions  
 261 can be chosen, so we keep the corresponding expressions general. Popular options may include a  
 262 linear component, an exponential component that saturates, and/or a power term. For the 3D for-  
 263 mulation, those scalar bounds, along with  $\dot{q}$ , shall be further multiplied by  $\sqrt{\frac{2}{3}}$  to obtain consistent  
 264 results.

265 A careful examination shows the boundary between subloading surface theory and conventional  
 266 plasticity is blurred. In specific, the following can be observed.

- 267 1. The term  $zF$  controls the effective size of the yield surface: during loading  $zF$  grows from 0  
 268 to  $F$ , so there is no initial elastic domain. It is possible to define a similar loading behaviour  
 269 in conventional plasticity by using an isotropic hardening function that starts from zero.
- 270 2. During unloading, the subloading surface contracts so the current stress point remains on the  
 271 surface. This can also be achieved in conventional plasticity by simply adjusting isotropic  
 272 hardening.
- 273 3. The term  $(1 - z) H_d \mathbf{d}$  acts as an additional, generalised back stress contribution, comple-  
 274 menting the conventional  $H_\alpha \boldsymbol{\alpha}$  term.

275 Without introducing any additional (memory) surfaces, Table 1 shows that the subloading surface  
 276 theory can be deemed as a generalisation of conventional plasticity, and it is effectively a single  
 277 surface theory. The proposed model mimics a balloon, expanding during loading and contracting  
 278 during unloading. It is thus denoted as the **balloon** model.

279 *3.7. Local System*

280 The overall implementation procedure follows the previous work [13]. Here we only emphasis  
 281 the changes brought by the proposed formulation. The local system consists of two residuals,  $f_s$   
 282 and  $z$ .

$$\mathbf{R} = \begin{cases} \|\boldsymbol{\eta}\| - zF, \\ F(z - z_n) - U\dot{q}. \end{cases} \quad (20)$$

283 Taking the local variable as  $\mathbf{x} = \begin{bmatrix} \gamma & z \end{bmatrix}^T$ , the Jacobian  $\mathbf{J}$  shall be written as

$$\mathbf{J} = \begin{bmatrix} \frac{\partial \|\boldsymbol{\eta}\|}{\partial \gamma} - z \frac{\partial F}{\partial \gamma} & \frac{\partial \|\boldsymbol{\eta}\|}{\partial z} - F - z \frac{\partial F}{\partial z} \\ \frac{\partial F}{\partial \gamma} (z - z_n) - U \frac{\partial \dot{q}}{\partial \gamma} - \dot{q} \frac{\partial U}{\partial \gamma} & \frac{\partial F}{\partial z} (z - z_n) + F - \dot{q} \frac{\partial U}{\partial z} \end{bmatrix}. \quad (21)$$

284 In the above, both  $F$  and  $U$  are functions of both  $z$  and  $\gamma$  via  $q_m$  and  $q_c$ . This differs from the  
 285 previous formulation [13].

286 **4. Numerical Examples**

287 We present a few numerical examples to demonstrate the capabilities of the proposed model.  
 288 For brevity, we mostly use normalised quantities in the following examples. In specific, stresses  
 289 are normalised by the initial yield stress, which is often the initial size of the conventional yield  
 290 surface; strains are normalised by the initial yield strain, which is the initial yield stress divided  
 291 by the elastic modulus. By such, the conventional yield point is always located at (1, 1).

292 For  $z_r$ , the average of the most recent a few (2 to 10)  $z_r^j$  values is used unless otherwise specified.  
 293 This choice appears to be random and ad hoc, but it works well in the numerical examples presented  
 294 here.

295 It's important to highlight that there is no goal to accurately adjust the model to match the  
 296 experimental data perfectly in the following examples. Rather, the emphasis is on showcasing the  
 297 adaptability of the suggested model in qualitatively representing different cyclic behaviour.

298 *4.1. Stiffness Degradation*

299 Fig. 4 demonstrates the gradual degradation of stiffness controlled by  $u$  during loading phases  
 300 where  $z$  increases. The following parameters/functions are used.

$$F = F_m = 1, \quad u = 100 \exp(-0.2q_m). \quad (22)$$

301 Since  $u$  effectively controls how fast  $z$  increases to unity, a smaller  $u$  leads to a slower transition. The  
 302 proposal § 3.4 does not rely on additional history variable, and implementing such a degradation  
 303 is straightforward. Alternatively, it is also possible to associate  $u$  with  $q$ , in which case such a  
 degradation would occur under cyclic loading as well. In other models, it is typically achieved by

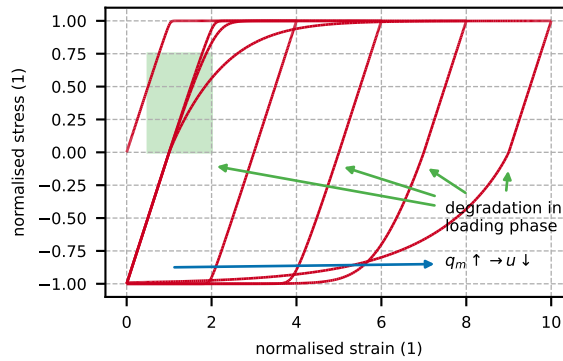


Figure 4: stiffness degradation controlled by  $u$

304  
 305 introducing a reduction factor for elastic modulus, or directly turning elastic modulus itself into a  
 306 history variable [e.g., 25].

307 It is also worth noting that  $H_d$  is defaulted to zero in this example to highlight the difference  
 308 between this proposal and other models, hence unloading phrases where  $z$  decreases are similar  
 309 to conventional models and exhibit a constant stiffness, viz., the initial elastic modulus. For real-  
 310 world implementations, setting  $H_d$  close to  $F$  effectively moves the similarity center toward the  
 311 boundary, thereby reducing the visual prominence of unloading regions.

312 *4.2. Isotropic Hardening Stagnation*

313 In the example shown in Fig. 5, isotropic hardening is fully deactivated during cyclic loading.  
 314 As a result, hysteresis loops stabilise immediately. The following configurations are used,

$$k_r = 100, \quad F = F_m = 1 + 0.05q_m. \quad (23)$$

315 In terms of  $z_r$ , the most recent  $z_r^j$  value at load reversal is used.

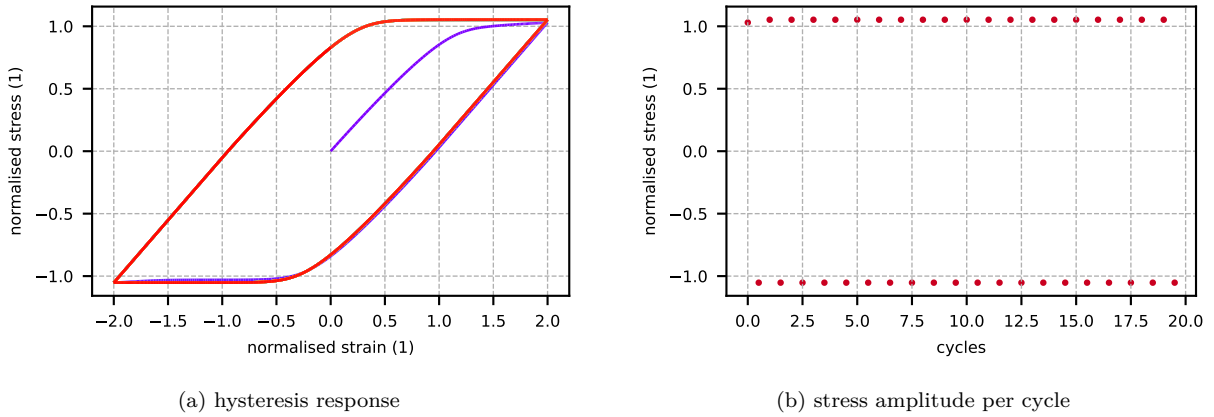


Figure 5: isotropic hardening stagnation

316 If one allows  $z_r$  to gradually increase by defining it to be the average of recent **a few**  $z_r^j$  values  
 317 at load reversals, even if under cyclical loadings with a fixed  $z$  magnitude, hysteresis loops would  
 318 stabilise gradually. This behaviour may vary if  $z_r$  is defined differently. Fig. 6 demonstrates such  
 an example by averaging the most recent 8 values.

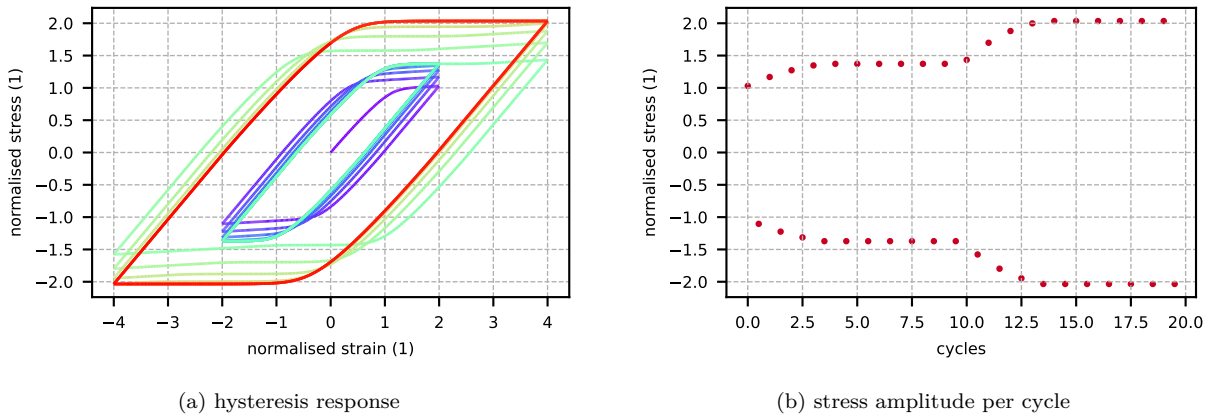


Figure 6: graduate isotropic hardening stagnation

320 4.3. Cyclic Hardening and Softening

321 The  $F_c$  component is dedicated to modelling cyclic hardening/softening. Fig. 7 shows an  
 322 example of cyclic hardening using the following expression for  $H_c$ .

$$H_c = 0.05q_m. \tag{24}$$

323 Since  $F_c$  does not evolve when  $z < z_r$ , the very first cycle thus sets an anchor value. Subsequent  
 324 loops would mostly contribute to  $q_c$  that gradually saturates  $F_c$  to  $H_c$ . This process repeats  
 whenever a new maximum  $q_m$  is reached and the hysteresis loops stabilise eventually. Noting that

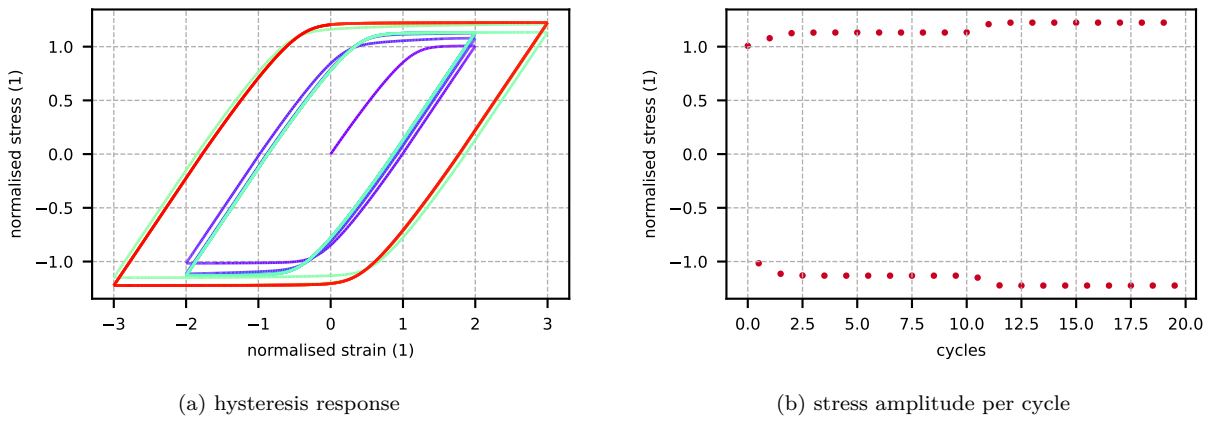


Figure 7: cyclic hardening

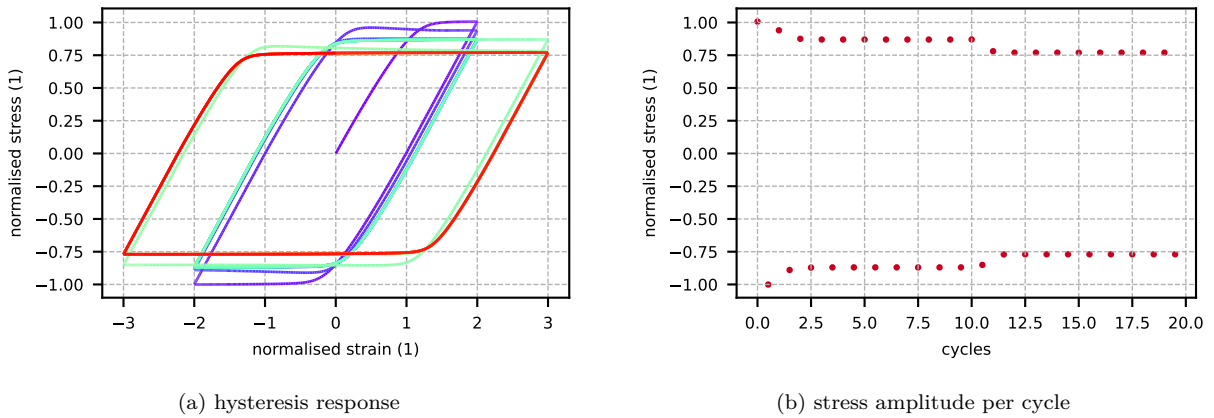


Figure 8: cyclic softening

325  
 326 there is no restriction on how  $H_c$  evolves, if  $H_c$  decreases with  $q_m$ , cyclic softening can be observed

327 as shown in Fig. 8, in which the following expression is used.

$$H_c = -0.05q_m. \quad (25)$$

328 However, for softening,  $z_r$  may stay unchanged after reaching unity, making subsequent softening  
 329 difficult if not impossible to achieve since Eq. (19) only accounts for the ‘relative’ load level instead  
 330 of the absolute one. If  $z_r$  has a short memory, e.g., depends on a limited number of recent  $z_r^j$  values,  
 331 it is possible to re-trigger softening by cycling at a relatively lower load level before returning to  
 332 a higher load level. However, whether such a behaviour is physically meaningful remains to be  
 333 investigated. It is also possible to refine the definitions of  $K_m$  and  $K_c$  to account for additional  
 334 factors, but this is not pursued here for brevity.

#### 335 4.4. SS304

The parameters/expressions used in this example are summarised in Table 2. SS304 exhibits

Table 2: model parameters/expressions for SS304

evolution of $z$	$u = 200 + 3800 \exp(-2000q_m)$
isotropic hardening $F_m$	$F_m = 0.2 + 2q_m$ (GPa)
isotropic hardening $F_c$	$F_c = 0.1 - 0.1 \exp(-100q_m)$ (GPa)
kinematic hardening	linear (Prager type) + exponential (AF type) saturation
similarity	$H_d = 0.8F$

336  
 337 cyclic hardening behaviour that is well captured by a saturating  $F_c$  component. Fig. 9 and Fig. 10  
 show the results of single step and multistep strain–symmetric cycling, respectively. The same set

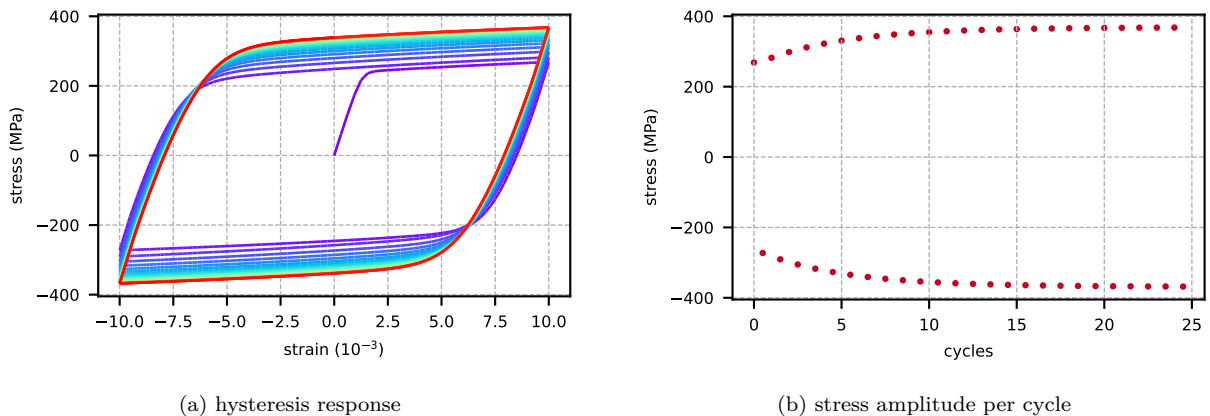


Figure 9: single step strain–symmetric cycling on SS304 [cf. 18, Fig. 2]

338

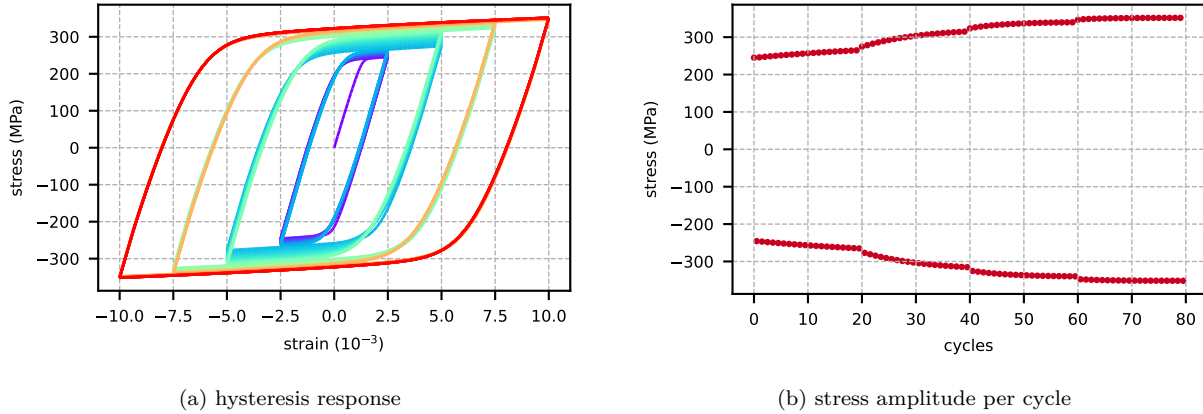


Figure 10: multistep strain-symmetric cycling on SS304 [cf. 18, Fig. 11]

339 of parameters can also capture satisfactory results for ratcheting under fixed stress/strain ampli-  
 340 tude. Fig. 11 shows both cases. Although the model successfully captures the overall characteristics  
 341 of the experimental data, the initial accumulation of plastic strain (or ratcheting strain) is overes-  
 342 timated relative to the experimental data as shown in Fig. 11a, indicating that further calibration  
 may be required for improved accuracy.

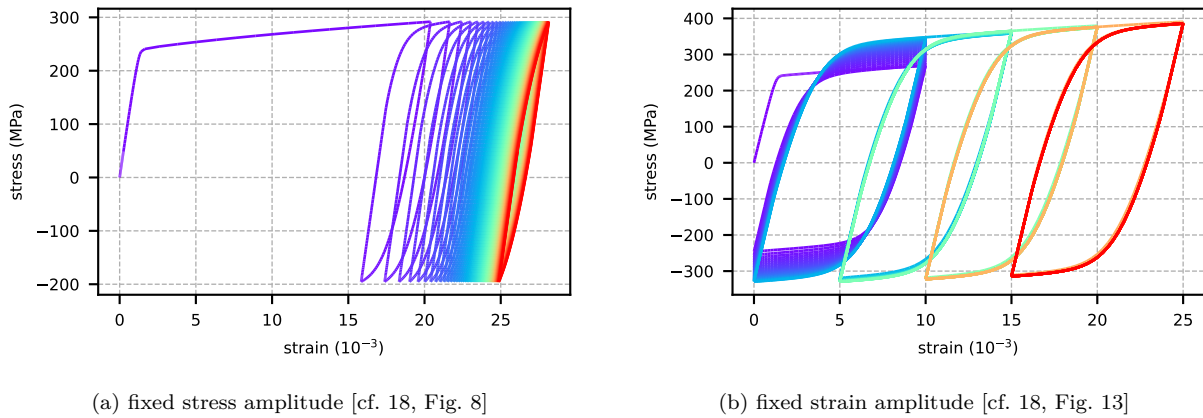


Figure 11: ratcheting of SS304

343

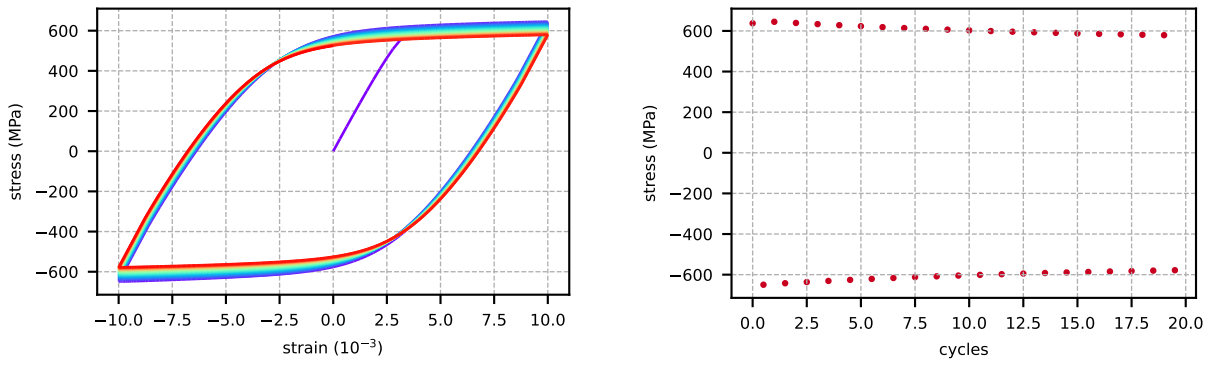
#### 344 4.5. CS1018

345 The parameters/expressions used in this example are summarised in Table 3. The experimental  
 346 results [18] show a significant correlation between the centre of stabilised hysteresis loops and  
 347 plastic history for CS1018 material. Thus, in this example, the kinematic hardening rule adopts  
 348 a combination of linear (Prager type) component and exponential (Armstrong-Frederick type)

Table 3: model parameters/expressions for CS1018

evolution of $z$	$u = 400 + 3600 \exp(-1000q_m)$
isotropic hardening $F_m$	$F_m = 0.6 + q_m$ (GPa)
isotropic hardening $F_c$	$F_c = -0.1 + 0.1 \exp(-100q_m)$ (GPa)
kinematic hardening	linear (Prager type) + exponential (AF type) saturation
similarity	$H_d = 0.8F$

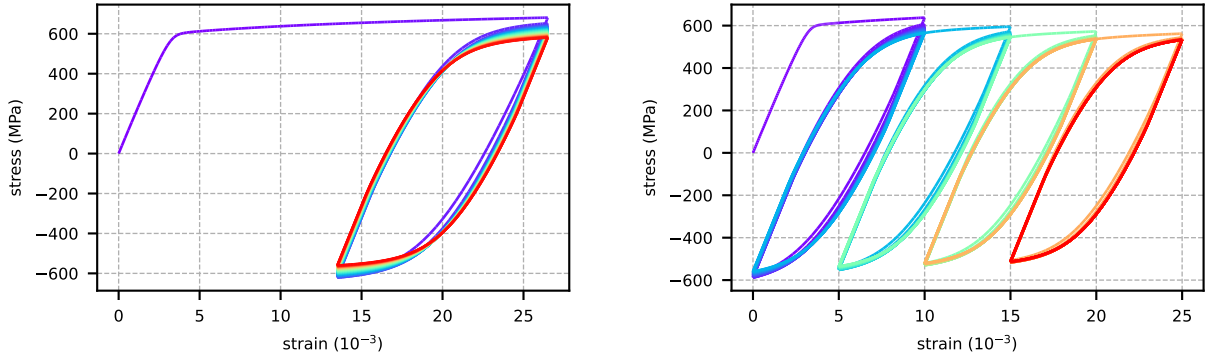
349 saturation component. By choosing a negative  $F_c$ , cycling within a fixed strain range leads to  
 cyclic softening.



(a) hysteresis response

(b) stress amplitude per cycle

Figure 12: cyclic softening of CS1018 [cf. 18, Fig. 3]



(a) single step

(b) multistep

Figure 13: strain controlled cycling of CS1018 [cf. 18, Figs. 4 and 12]

350

#### 351 4.6. Q345

352 The Q345 steel [see 25, 35] exhibits little to no cyclic hardening/softening. Hysteresis loops  
 353 stabilise immediately. One can simply set  $F_c = 0$ . Calibration is relatively straightforward. The

parameters/expressions used in this example are summarised in Table 4. Instead of using the mean

Table 4: model parameters/expressions for Q345

evolution of $z$	$u = 100 + 3900 \exp(-1000q_m)$
isotropic hardening $F_m$	$F_m = 0.33 + q_m$ (GPa)
isotropic hardening $F_c$	$F_c = 0$ (GPa)
kinematic hardening	linear (Prager type) + exponential (AF type) saturation
similarity	$H_d = 0.8F$

354

355 value of recent a few  $z$  values at load reversals, in this example, the maximum is used. Fig. 14 shows the hysteresis loops under two different loading protocols.

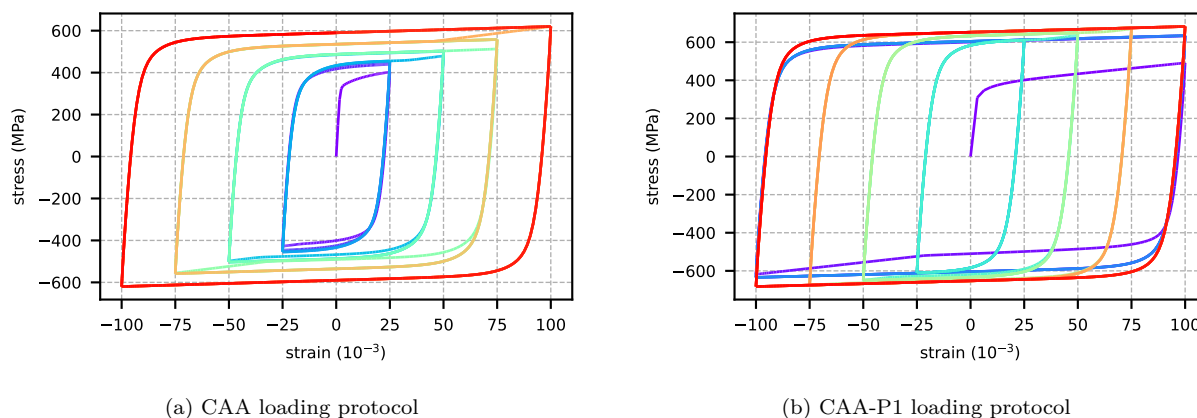


Figure 14: hysteresis loops of Q345 [cf. 25, Fig. 5]

356

## 357 5. Conclusions

358 In this work, we introduced the **Balloon-v1** model, a versatile constitutive framework for  
 359 accurately modeling the complex cyclic response of metallic materials. Built upon the foundation  
 360 of the subloading surface theory, the model achieves its enhanced capabilities without the need for  
 361 additional, computationally demanding memory surfaces.

362 The core innovation lies in a novel isotropic hardening formulation that is driven by an additive  
 363 decomposition of the plastic strain. This split allows the model to distinguish between plastic strain  
 364 accumulated during monotonic loading and that accumulated during cyclic loading. Leveraging  
 365 the loading reversal information inherently embedded in the normal yield ratio,  $z$ , this framework  
 366 enables the following key features.

367 • **Work/Isotropic Hardening Stagnation** By conditionally deactivating the evolution of  
368 the monotonic hardening component ( $F_m$ ) based on the current loading level relative to the  
369 history of load reversals ( $z_r$ ), the model effectively captures the stabilization of hysteresis  
370 loops.

371 • **Controllable Cyclic Hardening/Softening** The cyclic isotropic hardening component  
372 ( $F_c$ ) is dedicated to modeling this transient behaviour and can saturate in multiple stages,  
373 offering a refined response compared to other literature models.

374 The result is a streamlined and efficient formulation that is close to the original subloading  
375 surface model. Through a comprehensive set of numerical examples, including simulations of  
376 SS304, CS1018, and Q345, we demonstrated its robustness in capturing:

- 377 • stable hysteresis loops and stiffness degradation,
- 378 • isotropic hardening stagnation,
- 379 • cyclic hardening and softening,
- 380 • improved ratcheting response.

381 By providing an alternative to increasingly complex kinematic hardening law based approaches,  
382 the **Balloon-v1** model offers a powerful and numerically efficient tool for predictive simulations  
383 in metal plasticity. Future research will focus on extending the model’s application to multiaxial  
384 loading conditions and other complex cyclic phenomena such as the multi-stage ‘tertiary evolution  
385 of ratcheting’ [28]. Furthermore, the history of load reversals, as embedded in  $z_r$ , only adopts  
386 simple functions for the purpose of demonstration in this work. More sophisticated definitions can  
387 be explored to account for fatigue related phenomena in future studies.

388 Both the uniaxial (1D) and multiaxial (3D) versions of the proposed model are implemented  
389 in the open-source finite element analysis framework **suanPan** [36]. All numerical models and the  
390 relevant scripts are available in this repository<sup>2</sup>.

---

<sup>2</sup><https://github.com/TLCFEM/balloon-v1>

391 **References**

- 392 [1] S. Suresh, *Fatigue of Materials*, Cambridge University Press, 1998. doi:10.1017/  
393 cbo9780511806575.
- 394 [2] J. C. Simo, T. J. R. Hughes, *Computational Inelasticity*, Springer-Verlag, 1998. doi:10.1007/  
395 b98904.
- 396 [3] Y. F. Dafalias, E. P. Popov, A model of nonlinearly hardening materials for complex loading,  
397 *Acta Mechanica* 21 (1975) 173–192. doi:10.1007/bf01181053.
- 398 [4] R. D. Krieg, A practical two surface plasticity theory, *Journal of Applied Mechanics* 42 (1975)  
399 641–646. doi:10.1115/1.3423656.
- 400 [5] K. Hashiguchi, Constitutive equations of elastoplastic materials with elastic-plastic transition,  
401 *Journal of Applied Mechanics* 47 (1980) 266–272. doi:10.1115/1.3153653.
- 402 [6] K. Hashiguchi, Subloading surface model in unconventional plasticity, *International Journal*  
403 *of Solids and Structures* 25 (1989) 917–945. doi:10.1016/0020-7683(89)90038-3.
- 404 [7] K. Hashiguchi, M. Ueno, T. Anjiki, Subloading-overstress model: Unified constitutive equation  
405 for elasto-plastic and elasto-viscoplastic deformations under monotonic and cyclic loadings:  
406 Research with systematic review, *Archives of Computational Methods in Engineering* 30  
407 (2023) 2627–2649. doi:10.1007/s11831-022-09880-y.
- 408 [8] K. Hashiguchi, Y. Yamakawa, T. Anjiki, M. Ueno, Comprehensive review of subloading surface  
409 model: Governing law of irreversible mechanical phenomena of solids, *Archives of Computa-*  
410 *tional Methods in Engineering* 31 (2024) 1579–1609. doi:10.1007/s11831-023-10022-1.
- 411 [9] F. Yoshida, T. Uemori, A model of large-strain cyclic plasticity describing the bauschinger  
412 effect and workhardening stagnation, *International Journal of Plasticity* 18 (2002) 661–686.  
413 doi:10.1016/s0749-6419(01)00050-x.
- 414 [10] M. Mahan, Y. F. Dafalias, M. Taiebat, Y. Heo, S. K. Kunnath, Sanisteel: Simple anisotropic  
415 steel plasticity model, *Journal of Structural Engineering* 137 (2011) 185–194. doi:10.1061/  
416 (asce)st.1943-541x.0000297.

- 417 [11] K. Hashiguchi, *Foundations of Elastoplasticity: Subloading Surface Model*, 3rd ed., Springer  
418 International Publishing, 2017. doi:10.1007/978-3-319-48821-9.
- 419 [12] Y. F. Dafalias, E. P. Popov, Cyclic loading for materials with a vanishing elastic region,  
420 *Nuclear Engineering and Design* 41 (1977) 293–302. doi:10.1016/0029-5493(77)90117-0.
- 421 [13] T. L. Chang, On the subloading surface model for metals: some insights and an ef-  
422 ficient numerical implementation, *Acta Mechanica* 236 (2025) 3695–3717. doi:10.1007/  
423 s00707-025-04339-0.
- 424 [14] F. Yoshida, T. Uemori, K. Fujiwara, Elastic–plastic behavior of steel sheets under in-plane  
425 cyclic tension–compression at large strain, *International Journal of Plasticity* 18 (2002) 633–  
426 659. doi:10.1016/s0749-6419(01)00049-3.
- 427 [15] G. Kang, Q. Gao, L. Cai, Y. Sun, Experimental study on uniaxial and nonproportionally mul-  
428 ti-axial ratcheting of ss304 stainless steel at room and high temperatures, *Nuclear Engineering*  
429 *and Design* 216 (2002) 13–26. doi:10.1016/s0029-5493(02)00062-6.
- 430 [16] G. Kang, Q. Kan, J. Zhang, Y. Sun, Time-dependent ratchetting experiments of ss304 stainless  
431 steel, *International Journal of Plasticity* 22 (2006) 858–894. doi:10.1016/j.ijplas.2005.05.  
432 006.
- 433 [17] T. Hassan, S. Kyriakides, Ratcheting in cyclic plasticity, part i: Uniaxial behavior, *Interna-*  
434 *tional Journal of Plasticity* 8 (1992) 91–116. doi:10.1016/0749-6419(92)90040-j.
- 435 [18] T. Hassan, S. Kyriakides, Ratcheting of cyclically hardening and softening materials: I.  
436 uniaxial behavior, *International Journal of Plasticity* 10 (1994) 149–184. doi:10.1016/  
437 0749-6419(94)90033-7.
- 438 [19] T. Hassan, L. Taleb, S. Krishna, Influence of non-proportional loading on ratcheting responses  
439 and simulations by two recent cyclic plasticity models, *International Journal of Plasticity* 24  
440 (2008) 1863–1889. doi:10.1016/j.ijplas.2008.04.008.
- 441 [20] K. A. Meyer, J. Ahlström, The role of accumulated plasticity on yield surface evolution in  
442 pearlitic steel, *Mechanics of Materials* 179 (2023) 104582. doi:10.1016/j.mechmat.2023.  
443 104582.

- 444 [21] N. Ohno, A constitutive model of cyclic plasticity with a nonhardening strain region, *Journal*  
445 *of Applied Mechanics* 49 (1982) 721–727. doi:10.1115/1.3162603.
- 446 [22] J. Chaboche, A review of some plasticity and viscoplasticity constitutive theories, *International*  
447 *Journal of Plasticity* 24 (2008) 1642–1693. doi:10.1016/j.ijplas.2008.03.009.
- 448 [23] L. Xu, X. Nie, J. Fan, M. Tao, R. Ding, Cyclic hardening and softening behavior of the  
449 low yield point steel bly160: Experimental response and constitutive modeling, *International*  
450 *Journal of Plasticity* 78 (2016) 44–63. doi:10.1016/j.ijplas.2015.10.009.
- 451 [24] Z. Xie, A. Kanvinde, Y. Chen, A constitutive model for various structural steels considering  
452 shared hysteretic behaviors, *Journal of Constructional Steel Research* 176 (2021) 106421.  
453 doi:10.1016/j.jcsr.2020.106421.
- 454 [25] S. Zheng, R. Zhang, A novel constitutive model under various cyclic loading protocols with  
455 large strain ranges considering strain memory effect and loading history dependence, *International*  
456 *Journal of Fatigue* 202 (2026) 109239. doi:10.1016/j.ijfatigue.2025.109239.
- 457 [26] Q. Yang, W. Zhang, Y. Guo, F. Liang, P. Yin, L. Chang, C. Zhou, A universal constitutive  
458 model considering strain range dependence effect and transient behaviour for both cyclic  
459 softening and hardening steels, *Engineering Fracture Mechanics* 290 (2023) 109481. doi:10.  
460 1016/j.engfracmech.2023.109481.
- 461 [27] N. Ohno, J.-D. Wang, Kinematic hardening rules with critical state of dynamic recovery, part  
462 i: formulation and basic features for ratchetting behavior, *International Journal of Plasticity*  
463 9 (1993) 375–390. doi:10.1016/0749-6419(93)90042-o.
- 464 [28] G. Kang, Ratchetting: Recent progresses in phenomenon observation, constitutive model-  
465 ing and application, *International Journal of Fatigue* 30 (2008) 1448–1472. doi:10.1016/j.  
466 ijfatigue.2007.10.002.
- 467 [29] C. O. Frederick, P. J. Armstrong, A mathematical representation of the multiaxial baushinger  
468 effect, *Materials at High Temperatures* 24 (2007) 1–26. doi:10.3184/096034007x207589.
- 469 [30] F. Yoshida, A constitutive model of cyclic plasticity, *International Journal of Plasticity* 16  
470 (2000) 359–380. doi:10.1016/s0749-6419(99)00058-3.

- 471 [31] A. S. Semenov, B. E. Melnikov, Multisurface Theory of Plasticity with One Active Surface:  
472 Basic Relations, Experimental Validation and Microstructural Motivation, Springer Interna-  
473 tional Publishing, 2022, pp. 207–232. doi:10.1007/978-3-030-97675-0\_8.
- 474 [32] A. Ucak, P. Tsopelas, Constitutive model for cyclic response of structural steels with yield  
475 plateau, *Journal of Structural Engineering* 137 (2011) 195–206. doi:10.1061/(asce)st.  
476 1943-541x.0000287.
- 477 [33] A. Ucak, P. Tsopelas, Accurate modeling of the cyclic response of structural components  
478 constructed of steel with yield plateau, *Engineering Structures* 35 (2012) 272–280. doi:10.  
479 1016/j.engstruct.2011.10.015.
- 480 [34] F. Hu, G. Shi, Y. Shi, Constitutive model for full-range elasto-plastic behavior of structural  
481 steels with yield plateau: Formulation and implementation, *Engineering Structures* 171 (2018)  
482 1059–1070. doi:10.1016/j.engstruct.2016.02.037.
- 483 [35] Z. Xie, Y. Chen, Experimental and modeling study of uniaxial cyclic behaviors of struc-  
484 tural steel under ascending/descending strain amplitude-controlled loading, *Construction and*  
485 *Building Materials* 278 (2021) 122276. doi:10.1016/j.conbuildmat.2021.122276.
- 486 [36] T. L. Chang, suanpan — an open source, parallel and heterogeneous finite element analysis  
487 framework, 2024. doi:10.5281/ZENODO.13820988.